CERN-ATS-Note-2013-018 TECH

10th April 2013
rainer.wanzenberg@desy.de

Calculation of Wakefields and Higher Order Modes for the New Design of the Vacuum Chamber of the CMS Experiment for the HL-LHC

R. Wanzenberg and O. Zagorodnova
DESY, Notkestr. 85, 22603 Hamburg, Germany

Keywords: Wakefields, Higher Order Modes, CMS vacuum chamber, HL-LHC

Summary

To extend the discovery potential of the Large Hadron Collider (LHC) a design study for a novel machine configuration, the High Luminosity LHC (HL-LHC), was started with the goal to increase its luminosity by a factor of 10 beyond its design value. The new machine configuration will also include an upgraded detector configuration and a new beam pipe in the CMS detector. The short range wakefields and the trapped Higher Order Modes (HOMs) for the new design of the vacuum chamber are calculated and compared with the presently used chamber. The kick and loss parameters are presented for different sets of beam parameters. The numerical calculations have been performed with the computer codes MAFIA and ECHO2D. The obtained data are intended to be included into the impedance database of the HL-LHC.

The HiLumi LHC Design Study is included in the High Luminosity LHC project and is partly funded by the European Commission within the Framework Programme 7 Capacities Specific Programme, Grant Agreement 284404.

1 Introduction

1.1 The LHC accelerator

The Large Hadron Collider (LHC) [1, 2], which is installed in the 27 km long tunnel that had been previously been for the Large Electron Positron collider

(LEP), is the world's largest particle collider. The LHC has an 8-fold symmetry with eight arc sections and eight straight sections which contain experiments and systems for the machine operation. The two counter circulating proton beams collide at the interaction points (IPs) in sectors 1 and 5, where the experiments ATLAS (IP 1) and CMS (IP 5) have been installed.

The commissioning with proton beams started in September 2008 and was resumed at the end of 2009 after a severe failure of the bus-bar of a dipole magnet which required extensive repair work. Both proton beams with a beam energy of 3.5 TeV were successfully brought into collision in March 2010. In 2011 the LHC has delivered an integrated luminosity of 5.5 fb^{-1} to the ATLAS experiment and 5.7 fb^{-1} at a center of mass energy of 7 TeV. In 2012 the luminosity runs were successfully continued with a beam energy of 4.0 TeV.

The nominal parameters of the LHC for luminosity operation are summarized in Table 1, see Ref. [2].

Parameter	Symbol	Value	Unit
Proton energy	E_p	7000	GeV
Ring circumference	C_R	26658.883	m
Revolution frequency	f_R	11.245	kHz
Transverse normalized emittance	$\gamma\epsilon_{x,y}$	3.75	mm mrad
RMS bunch length	σ_z	7.55	cm
Half crossing angle at IP1 and IP5	$\theta_{1/2}$	142.5	μrad
Beta function at IP1 and IP5	$\beta^\star$	0.55	m
RMS beam size at IP1 and IP5	$\sigma_{x,y}$	16.7	μm
Peak luminosity in IP1 and IP5	$\hat{\mathcal{L}}$	$1.0 \cdot 10^{34}$	$\text{cm}^{-2}\ \text{s}^{-1}$
Number of bunches	N_b	2808	
Bunch spacing	Δt_b	25	ns
Number of particles per bunch	N_0	$1.15 \cdot 10^{11}$	
Charge of one bunch	q_b	18.4	nC
Circulating beam current	I_{tot}	0.582	A

Table 1: Nominal design parameters of the LHC at collision energy [2].

To extend the discovery potential of the LHC a design study for a upgraded machine configuration, the High Luminosity LHC (HL-LHC), was started in 2011, with the goal to increase its luminosity by a factor of 10 beyond its design value. The new machine configuration will also include an upgraded detector configuration and a new beam pipe in the CMS detector. The wakefields and higher order modes of this new vacuum chamber are considered in this report. Two possible parameter lists with different single bunch intensities for the HL-LHC are shown in Table 2.

Parameter	Option 1	Option 2	
Proton energy	7	7	TeV
Transverse normalized emittance	2.5	3.0	mm mrad
RMS bunch length	7.5	7.5	cm
Number of bunches	2808	1404	
Bunch spacing	25	50	ns
Number of particles per bunch	$2.2 \cdot 10^{11}$	$3.5 \cdot 10^{11}$	
Charge of one bunch	35.2	56.1	nC
Circulating beam current	1.11	0.89	A

Table 2: Two design parameters under consideration for the HL-LHC. A parameter set with a RMS bunch length of 4.0 cm is also being considered.

1.2 The CMS vacuum chamber

Inside of the CMS (Compact Muon Solenoid) experiment a vacuum chamber is installed which is matched to the needs of the installed detector components. A 3D-view of the presently installed vacuum system is shown in Fig. 1. Wakefields and HOMs for the present version and for older designs of the CMS vacuum chamber are presented in [3, 4, 5, 6, 7, 8]. For the HL-LHC it is foreseen to use a central beam pipe with a smaller diameter while the general layout of the chamber is similar to the presently installed chamber (Fig. 1). A schematic view of the new chamber is shown in Fig. 2. The angle of the tapered cone is unchanged in the new design. The geometry of the CMS chamber is a cylindrically symmetric

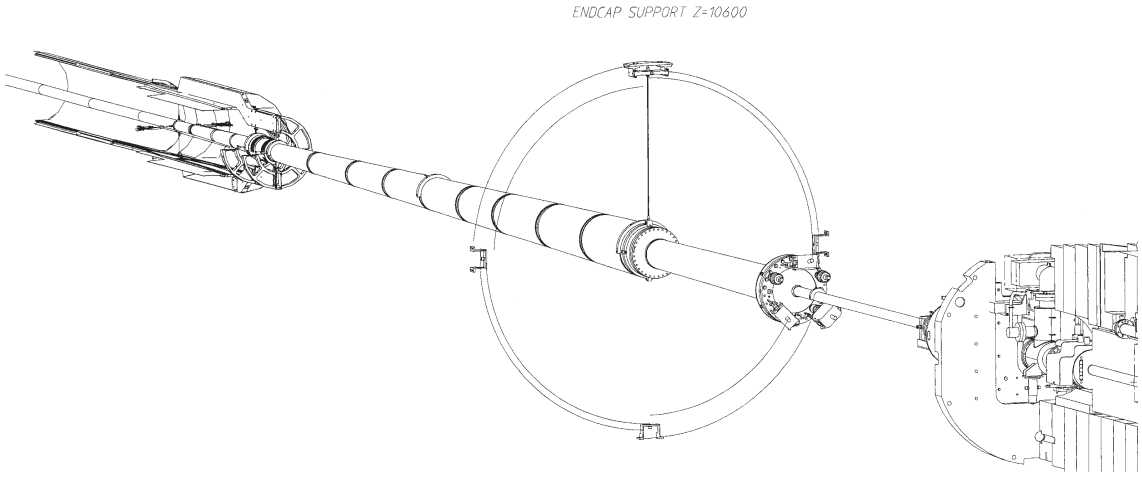

Figure 1: A 3D view of the presently installed CMS vacuum chamber. The beam pipe is shown from the interaction point to the compensation module.

structure. A list of the the r-z coordinates of the chamber is given in Table 3. A plot of the of r-z coordinates is shown in Fig. 3.

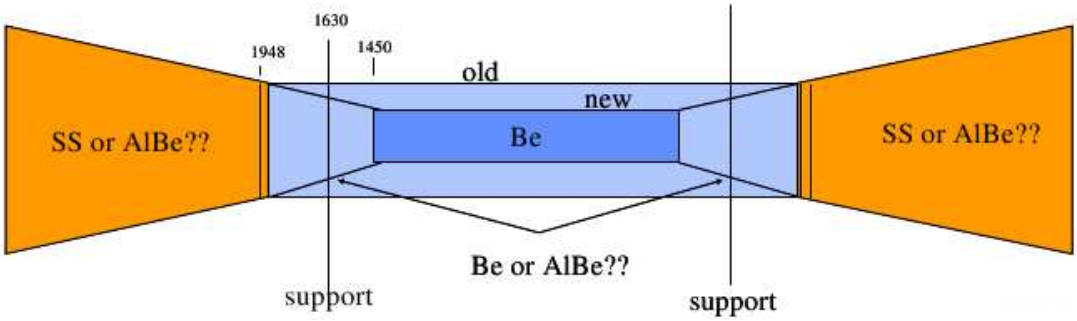

Figure 2: A schematic view of the new CMS vacuum chamber [9].

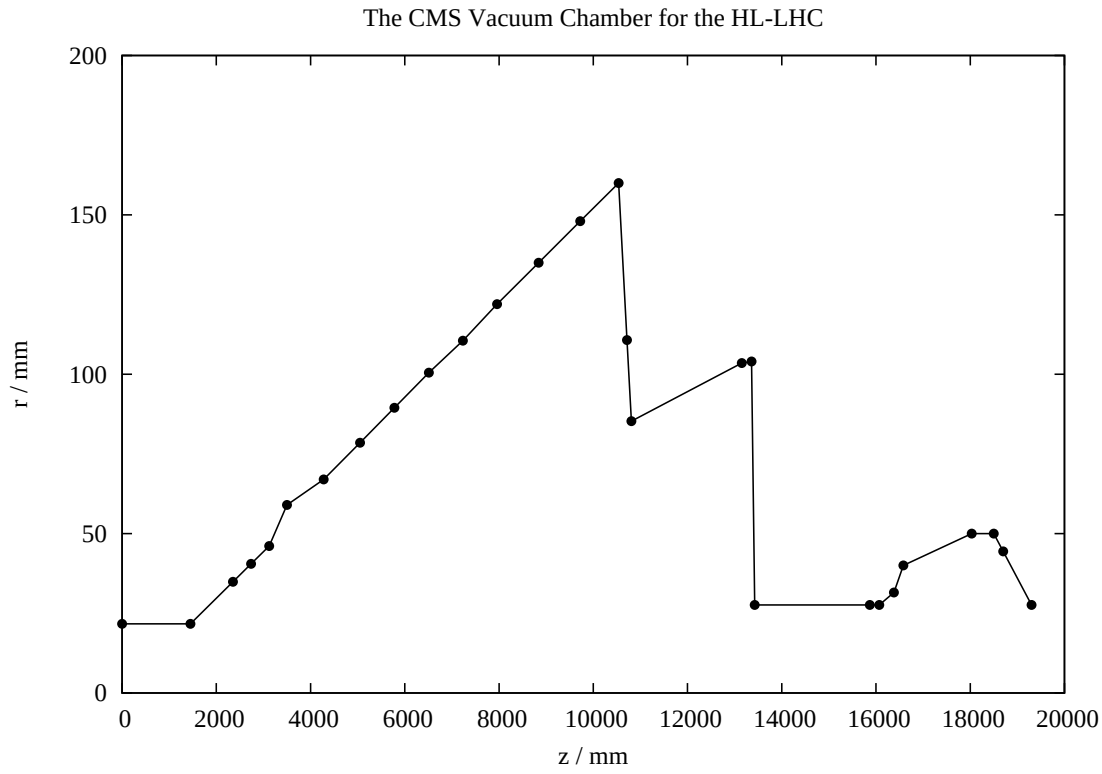

Figure 3: A representation of the vacuum chamber of the CMS experiment for the HL-LHC in r-z-coordinates. The vacuum chamber has a rotational symmetry along the z axis. All dimensions are in mm. The interaction point (IP) is at $z = 0$ mm. The marked points correspond to the positions in Table 3.

Name		z / mm	r /mm	Material	Cu 0.1μm	RF-shield
CP	1	0.0	**21.7**	Be	no	
	2	**1450.0**	**21.7**	Be or BeAl	no	
	3	2353.6	34.9	Steel	no	
	4	2736.6	40.5	Steel	no	
	5	3120.0	46.1	Steel	no	
EC	6	3500.0	59.0	Steel	yes	
	7	4279.0	67.0	Steel	yes	
	8	5049.0	78.5	Steel	yes	
	9	5779.0	89.5	Steel	yes	
	10	6510.0	100.5	Steel	yes	
	11	7234.0	110.5	Steel	no	
	12	7959.0	122.0	Steel	no	
	13	8841.0	135.0	Steel	no	
	14	9723.0	148.0	Steel	no	
	15	10538.0	160.0	Steel	no	
	16	10715.0	110.7	Steel	no	
HF	17	10809.0	85.3	Steel	yes	
	18	13152.0	103.5	Steel	yes	
	19	13359.0	104.0	Steel	no	yes
CT2	20	13427.0	27.6	Steel	no	yes
	21	15870.0	27.6	Steel	yes	
	22	16070.0	27.6	Steel	yes	
CM	23	16380.0	31.5	Steel	no	yes
FP	24	16580.0	40.0	Steel	yes	
	25	18030.0	50.0	Steel	yes	
Pump	26	18500.0	50.0		no	yes
Bellow	27	18700.0	44.4		no	yes
Trans	28	19300.0	27.6		yes	
CP	=Central Pipe					
EC	=End-cap Pipe					
HF	=HF (Hadron forward) Pipe					
CT2	=CT2 Pipe					
CM	=Compensation Module					
FP	=Forward Pipe					
Pump	=Vacuum pump					
Trans	=Transition Module					

Table 3: The main components of the new CMS vacuum system. The longitudinal position z measured from the IP and the radial dimensions are listed as well as the material properties.

2 Wakefields

2.1 Definitions and Numerical Calculations

Since the CMS vacuum chamber is rotationally symmetric with respect to the longitudinal axis it is convenient to use a two dimensional (r, z) computer code for numerical wakefield calculations. The ECHO2D code [10, 11] was used to calculate the Monopole and Dipole wakefields of the chamber. The geometry is shown in Fig. 4.

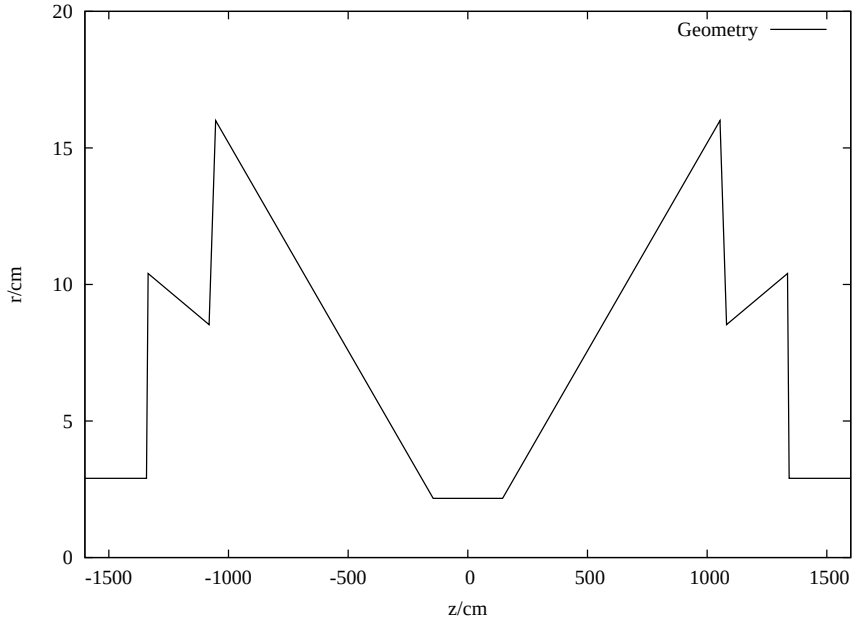

Figure 4: A schematic representation of the ECHO2D model of the CMS vacuum chamber. All dimensions are in mm. The interaction point (IP) is at $z = 0$ mm.

The wake potential [12] of a bunch with a charge q_1 is defined as:

$$\boldsymbol{W}(\boldsymbol{r}_{\perp 2}, \boldsymbol{r}_{\perp 1}, s) = \frac{1}{q_1} \int_0^L dz (\boldsymbol{E} + c\, \boldsymbol{e_z} \times \boldsymbol{B})_{t=(z+s)/c}. \tag{1}$$

The wake potential may be regarded as an average of the Lorentz force on a test charge q_2. $\boldsymbol{r}_{\perp 1}$ and $\boldsymbol{r}_{\perp 2}$ are the transverse coordinates of the bunch with charge q_1 and the test charge q_2. Causality requires $\boldsymbol{W}(s) = 0$ in front of the bunch[1]. The distance s is positive in the direction opposite to the motion of the bunch with charge q_1.

[1] This is strictly true for ultra relativistic bunches ($v = c$ or $\beta = 1$). For the LHC beam it is a very good approximation.

The longitudinal and transverse components of the wake potential are connected by the Panofsky–Wenzel theorem [13]

$$\frac{\partial}{\partial s}\boldsymbol{W}_{\perp}(\boldsymbol{r}_{\perp 2}, \boldsymbol{r}_{\perp 1}, s) = -\boldsymbol{\nabla}_{\perp_2} W_{\parallel}(\boldsymbol{r}_{\perp 2}, \boldsymbol{r}_{\perp 1}, s). \tag{2}$$

Integration of the transverse gradient (applied to the transverse coordinates of the test charge) of the longitudinal wake potential yields the transverse wake potential. If the structure traversed by the bunch is cylindrically symmetric then a multipole expansion can be used to describe the wake potential. The longitudinal wake potential is given by:

$$W_{\parallel}(r_1, r_2, \varphi_1, \varphi_2, s) = \sum_{m=0}^{\infty} {r_1}^m \, {r_2}^m \; W_{\parallel}^{(m)}(s) \;\; \cos m\,(\varphi_2 - \varphi_1). \tag{3}$$

The functions $W_{\parallel}^{(m)}(s)$ are the longitudinal m-pole wake potentials. It is often sufficient to consider only the leading terms of the series in equation (3), neglecting contributions from quadrupole and higher multipole components. The transverse wake potential can be calculated using the Panofsky–Wenzel theorem:

$$W_{\perp}^{(m)}(s) = -\int_{-\infty}^{s} d\zeta \, W_{\parallel}^{(m)}(\zeta), \tag{4}$$

for $m > 0$. There is no transverse monopole wake potential. The dipole wake potential does not depend on the position of the test charge q_2. The kick on the test charge is linear in the offset of the point charge q_1.

Computer codes are used to calculate the wake potential for a Gaussian bunch with charge density

$$\rho(z) = q_b \, g(z), \;\; \text{with} \;\; g(z) = \frac{1}{\sigma_z} \frac{1}{\sqrt{2\,\pi}} \exp\left(-\frac{1}{2}\left(\frac{z}{\sigma_z}\right)^2\right). \tag{5}$$

q_b is the total charge of the bunch. A basic criteria to ensure a small numerical error of the results from wakefield calculation is [14]:

$$\frac{\Delta z^2 \, l}{{\sigma_z}^3} < 1, \tag{6}$$

where Δz is the step size, σ_z the rms bunch length and l is the total length of the vacuum chamber. For the CMS vacuum chamber the total length is about 32 m and the rms bunch length is 7.5 cm. The criteria (6) is fulfilled if a step size of $\Delta z = 2$ mm is used. In the radial direction a step size of $\Delta r = 1$ mm or even smaller was used to obtain a good mesh model of the small beam pipe in the center of the CMS chamber. Calculations for a short bunch of only 4.0 cm require an even smaller step size.

2.2 Loss and Kick Parameters

The numerical calculations provide the monopole and dipole wake potentials $W_{\parallel}^{(0)}(s)$ and $W_{\perp}^{(1)}(s)$. From the wake potentials the loss and kick parameters are obtained which are closely related to the impedance.

The total loss parameter is

$$k_{||\mathrm{tot}}^{(0)} = \int ds\; W_{\parallel}^{(0)}(s)\; g(s)\;, \tag{7}$$

where $g(s)$ is the normalized charge density of the bunch, see Eqn.(5). The total loss parameter $k_{\parallel\mathrm{tot}}^{(0)}$ characterizes the resistive part of the impedance and is closely related to the transient[2] power loss P of the beam:

$$P = N_b\, f_R\, {q_b}^2\, k_{||\mathrm{tot}}^{(0)}, \tag{8}$$

where N_b is the total number of bunches and q_b the single bunch charge, and f_R the revolution frequency (see Table 1).

The total (dipole) kick parameter is

$$k_{\perp}^{(1)} = \int ds\; W_{\perp}^{(1)}(s)\; g(s) \tag{9}$$

which is closely related to the transverse impedance (see [15])

$$(Z_{\perp})_{\mathrm{eff}} = 2\,\sqrt{\pi}\,\frac{\sigma_z}{c}\,k_{\perp}^{(1)}. \tag{10}$$

Furthermore it is possible to estimate the intensity dependent betatron tune shift:

$$\Delta\nu \approx q_b \frac{\langle\beta\rangle}{4\,\pi\,E_p/e}\,k_{\perp}^{(1)}, \tag{11}$$

where q_b is the single bunch charge, E_p is the beam energy, e is the charge of the proton and $\langle\beta\rangle$ is the average beta function in the CMS vacuum chamber.

The inductive part of the longitudinal impedance can be calculated from the averaged gradient of the wake potential of a Gaussian bunch:

$$\begin{aligned} k^{(0)}(1)_{\parallel\mathrm{tot}} &= \int ds\; \frac{d}{ds} W_{\parallel}^{(0)}(s)\; g(s) \\ &= -\int ds\; W_{\parallel}^{(0)}(s)\; \frac{d}{ds} g(s). \end{aligned} \tag{12}$$

The (minus) imaginary part of the effective longitudinal impedance is approximately

$$\left(-\Im[Z_{\parallel}]/n\right)_{\mathrm{eff}} \approx \omega_0\, 4\,\sqrt{\pi}\,\frac{{\sigma_z}^3}{c^2}\,k^{(0)}(1)_{\parallel\mathrm{tot}} \tag{13}$$

where $\omega_0 = 2\,\pi\,11.245\,\mathrm{kHz}$ is the revolution frequency of the LHC and $n = \omega/\omega_0$. The equation (13) is based on the assumption that the longitudinal (monopole) impedance can be approximated for small frequencies ω as $Z_{\parallel}(\omega) \approx -i\,\omega\,L$ with an inductance L, see also [16].

[2]The resonant power loss into one mode is discussed in the section about HOMs.

2.3 Results

The wake potentials have been calculated with the ECHO2D code using different step sizes and bunch lengths. Initially the same step size of $\Delta z = 2$ mm and of $\Delta r = 1$ mm as in Ref. [7] was used. Plots of the longitudinal *monopole* and transverse *dipole* wake potentials are shown in Fig. 5, Fig. 6 and Fig. 7 for a bunch length of $\sigma_z = 7.5$ cm. The results for the loss and kick parameters are summarized in Table 4.

Parameter	New chamber	Present chamber	Δz/cm	Δr/cm
$k^{(0)}_{\|\|\mathrm{tot}}$ (V/nC)	2.36	2.36	0.2	0.1
$k^{(1)}_{\perp}$ (V/pCm)	2.38	2.36	0.2	0.1

Table 4: Results for the loss and kick parameters for a Gaussian bunch with rms bunch length of $\sigma_z = 7.5$ cm. The results for the present chamber are obtained for the geometry in Ref. [7]

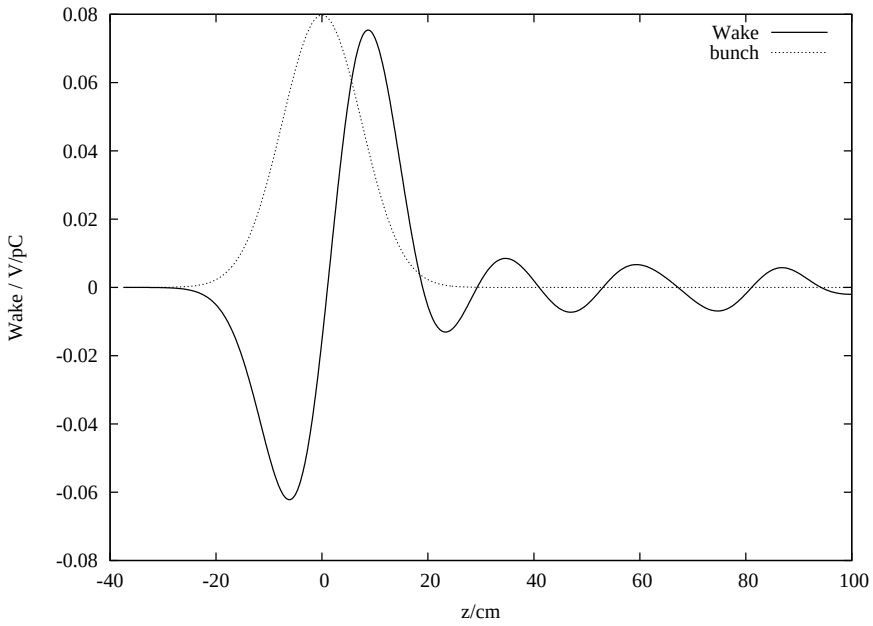

Figure 5: The longitudinal (monopole) wake potential of the CMS vacuum chamber. The wake has been calculated with the ECHO2D code for an rms bunch length of 7.5 cm. The bunch shape is also shown (in arbitrary units).

The results for the loss parameter for the new and present chambers do not differ within the numerical accuracy of the calculations. The kick parameter of 2.38 V/pCm for the new design is a bit larger than the corresponding parameter for the present chamber. The kick parameter corresponds to an effective

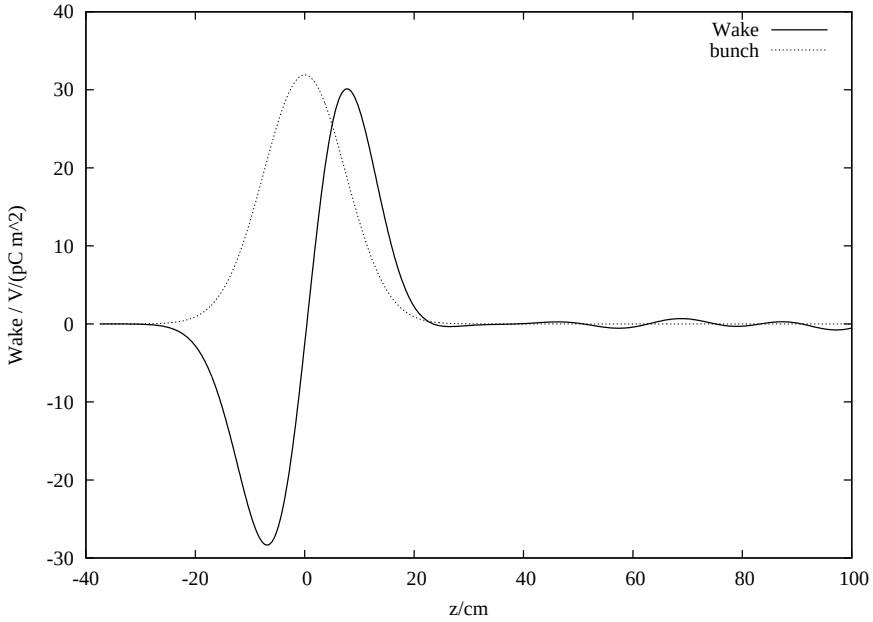

Figure 6: The longitudinal dipole wake potential of the CMS vacuum chamber. The wake has been calculated with the ECHO2D code for an rms bunch length of 7.5 cm. The bunch shape is also shown (in arbitrary units).

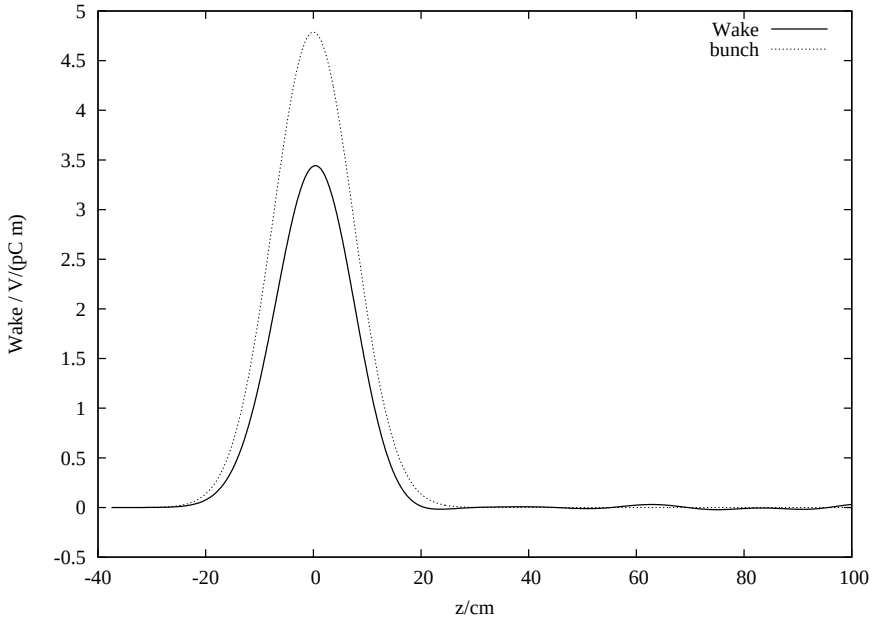

Figure 7: The transverse dipole wake potential of the CMS vacuum chamber. The wake has been calculated with the ECHO2D code for an rms bunch length of 7.5 cm. The bunch shape is also shown (in arbitrary units).

transverse impedance [3] (Eqn. (10)) of 2.1 kΩ/m. From the loss parameter of 2.36 V/nC one obtains a total transient power loss of about 92 W for Option 1 and of 117 W for Option 2 of the LHC-HL parameters, see table 2.

The average gradient of the longitudinal wake potential $k^{(0)}(1)_{\|\mathrm{tot}}$ is 0.508 V/pCm which corresponds to an effective impedance $\left(-\Im[Z_\|]/n\right)_{\mathrm{eff}}$ of $1.19{\cdot}10^{-3}\ \Omega$ according to Eqn. (13).

The calculations were repeated with very small step sizes of $\Delta z = 0.15$ cm, $\Delta r = 0.01$ cm for the longitudinal wake, and with step sizes of $\Delta z = 0.1$ cm, $\Delta r = 0.01$ cm for the transverse wake. The calculations have been done for a bunch length of $\sigma_z = 7.5$ cm and additionally for a bunch length of $\sigma_z = 4$ cm. The results for the loss and kick parameters are summarized in Table 5 for $\sigma_z = 7.5$ cm and in Table 6 for $\sigma_z = 4$ cm. The longitudinal loss parameter for the short bunch[4] ($\sigma_z = 4$ cm) is about a factor 19 larger than the loss parameter for the bunch with a length of $\sigma_z = 7.5$ cm. The total transient power loss of the beam is 2.2 kW for the parameter Option 2 of table 2, which may cause problems. The transverse kick parameter for the short bunch is about a factor 2 larger than the kick parameter for the $\sigma_z = 7.5$ cm bunch.

Parameter	New chamber	Present chamber	Δz/cm	Δr/cm
$k^{(0)}_{\|\mathrm{tot}}$ (V/nC)	2.35	2.35	0.15	0.01
$k^{(1)}_{\perp}$ (V/pCm)	2.38	2.35	0.1	0.01

Table 5: Results for the loss and kick parameters for a Gaussian bunch with rms bunch length of $\sigma_z = 7.5$ cm.

Parameter	New chamber	Present chamber	Δz/cm	Δr/cm
$k^{(0)}_{\|\mathrm{tot}}$ (V/nC)	45.5	45.5	0.15	0.01
$k^{(1)}_{\perp}$ (V/pCm)	4.62	4.56	0.1	0.01

Table 6: Results for the loss and kick parameters for a Gaussian bunch with rms bunch length of $\sigma_z = 4$ cm.

The total loss parameter has been calculated for several rms bunch lengths between 4.0 cm and 8.0 cm using a mesh with a step size of $\Delta z = \Delta r = 0.1\,$cm. The results are plotted in Fig. 8 (diamonds). The numerical results can be

[3] The effective transverse impedance is closely related to the imaginary part of the transverse impedance [15]: $(Z_\perp)_{\mathrm{eff}} = \frac{\sigma_z}{c\sqrt{\pi}} \int_{-\infty}^{\infty} d\omega\, \Im[Z_\perp(\omega)]\, \exp(-\omega^2\, {\sigma_z}^2/c^2)$.

[4] The criteria to ensure a small numerical error (see Eqn. (6)) is almost fulfilled for the step size of $\Delta z = 1.5\,$mm.

approximately fitted to a scaling law as

$$k^{(0)}_{||\mathrm{tot}}(\sigma_z) \approx k^{(0)}_{||\mathrm{tot}}(7.5\,\mathrm{cm}) \left(\frac{7.5\,\mathrm{cm}}{\sigma_z}\right)^{4.8}. \tag{14}$$

The corresponding curve is also shown in Fig. 8. The total loss parameter can also be written as

$$k^{(0)}_{||\mathrm{tot}} = \frac{1}{\pi}\int_0^\infty d\omega\; h(\omega)\,\Re(Z_\parallel)(\omega), \tag{15}$$

where $h(\omega) = \exp\left(-\left(\frac{\sigma_z}{c}\omega\right)^2\right)$ is the spectral power density of the bunch and $Z_\parallel$ is the longitudinal impedance. The characteristic bunch frequency $\omega_b = c/\sigma_z$ is $2\,\pi\,\cdot\,0.636\,\mathrm{GHz}$ for a rms bunch length of 4.0 cm and $2\,\pi\,\cdot\,1.193\,\mathrm{GHz}$ for a rms bunch length of 7.5 cm. The scaling law from Eqn. (14) indicates that the real part of the longitudinal is significantly contributing to the to loss parameter in the frequency range from 0.636 GHz to 1.193 GHz for a rms bunch length of 4.0 cm.

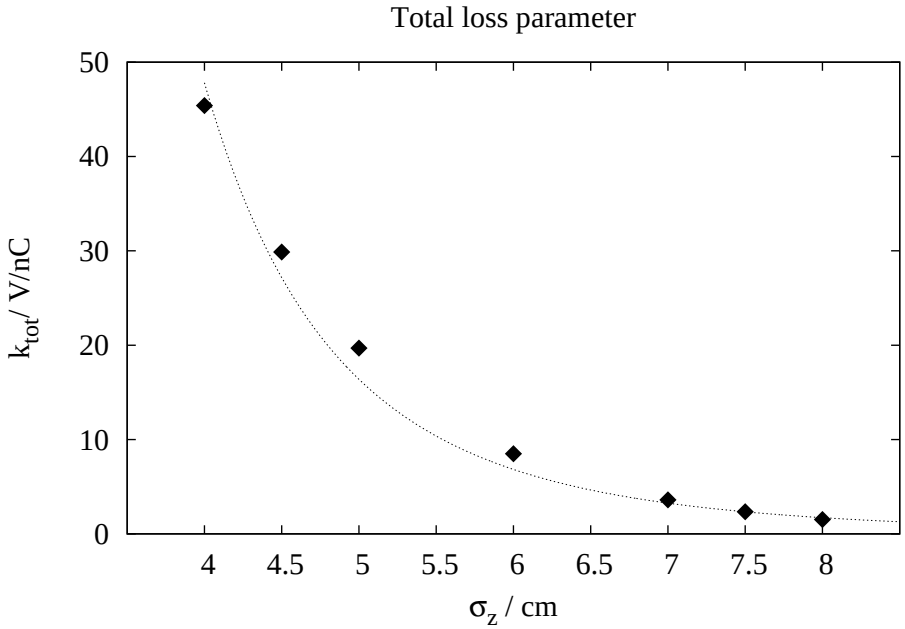

Figure 8: Total loss parameter versus rms bunch length for the CMS vacuum chamber.

Plots of the longitudinal *monopole* and transverse *dipole* wake potentials for a bunch length of $\sigma_z = 7.5$ cm are shown in Fig. 9 and Fig. 10. Plots of the longitudinal *monopole* and transverse *dipole* wake potentials for a bunch length of $\sigma_z = 4$ cm are shown in Fig. 11 and Fig. 12.

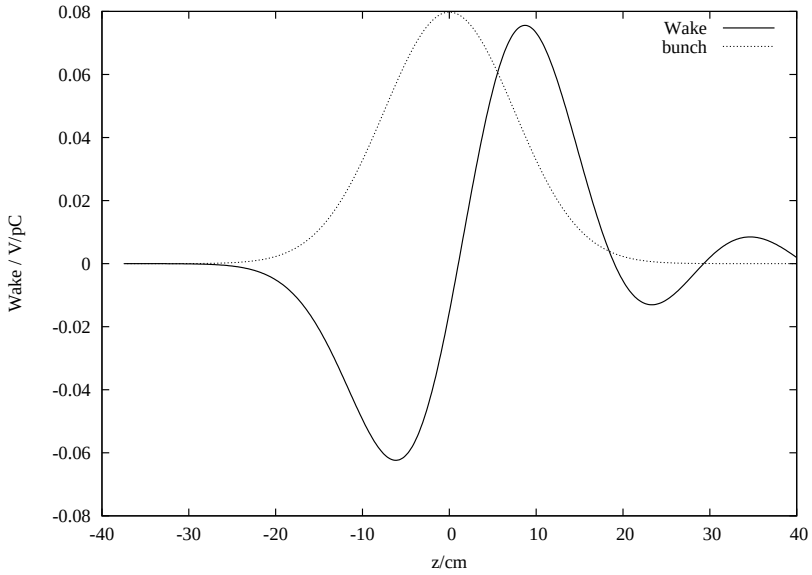

Figure 9: The longitudinal (monopole) wake potential of the CMS vacuum chamber. The wake has been calculated with the ECHO2D code for an rms bunch length of 7.5 cm using step sizes of $\Delta z = 0.15$ cm, $\Delta r = 0.01$ cm. The bunch shape is also shown (in arbitrary units).

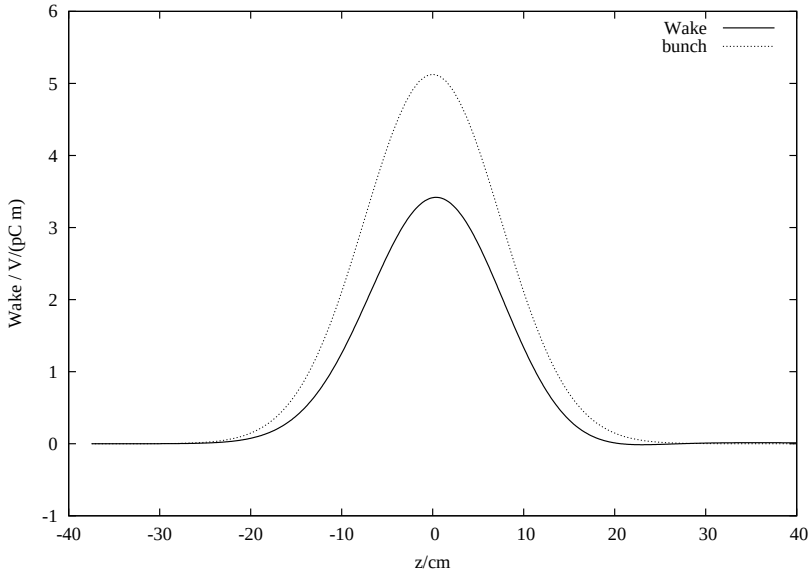

Figure 10: The transverse (dipole) wake potential of the CMS vacuum chamber. The wake has been calculated with the ECHO2D code for an rms bunch length of 7.5 cm using step sizes of $\Delta z = 0.1$ cm, $\Delta r = 0.01$ cm. The bunch shape is also shown (in arbitrary units).

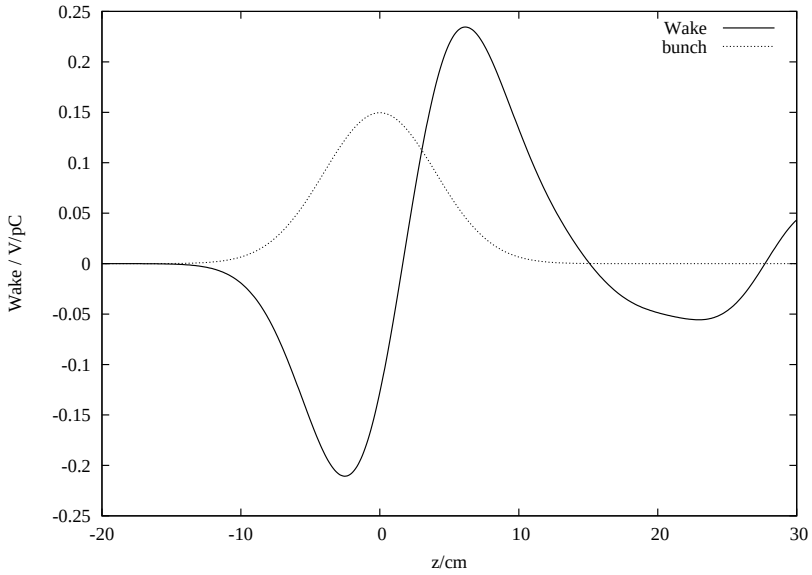

Figure 11: The longitudinal (monopole) wake potential of the CMS vacuum chamber. The wake has been calculated with the ECHO2D code for an rms bunch length of 4 cm using step sizes of $\Delta z = 0.15$ cm, $\Delta r = 0.01$ cm. The bunch shape is also shown (in arbitrary units).

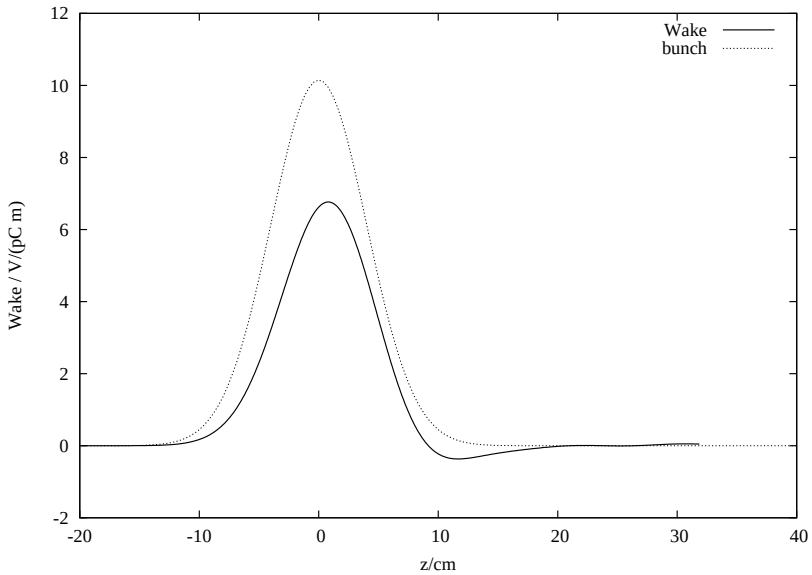

Figure 12: The transverse (dipole) wake potential of the CMS vacuum chamber. The wake has been calculated with the ECHO2D code for an rms bunch length of 4 cm using step sizes of $\Delta z = 0.1$ cm, $\Delta r = 0.01$ cm. The bunch shape is also shown (in arbitrary units).

3 Higher Order Modes - HOMs

The electric and magnetic fields of the higher order modes are calculated with the frequency domain solver of the computer code MAFIA [17, 18, 19]. A 2-dimensional model of the CMS vacuum chamber has been used since it is sufficient to model a cylindrically symmetric structure on a $r-z$-grid to obtain all important rf-parameters. For the calculations a simplified geometric model as shown in Fig. 4 has been used. Actually only the right half (0 m to 16 m) of the structure is modeled for the frequency domain calculations. For the calculations a mesh with step sizes of 1 mm in the radial (r) and 2 mm in the longitudinal (z) direction has been used. Electric (E) boundary conditions were used at both ends of the modeled structure. The MAFIA eigenvalue solver was used to calculate monopole and dipole modes. The modes are labeled as "EE-n" according to the boundary conditions at both ends and the mode number n, starting with the label "EE-1" for the mode with the lowest frequency.

The eigenvalue solver provides the frequency and the electric and magnetic fields for each mode on the mesh. For each mode the post-processing follows the scheme:

- Numerical Solution of the Maxwell Equations
  - Mode frequency $f = \omega/(2\,\pi)$
  - Electric and magnetic fields $\boldsymbol{E}$, $\boldsymbol{B}$
- Basic post processing
  - U stored energy in $\boldsymbol{E}$, $\boldsymbol{B}$ field of the mode
  - $V(r) = \int dz\, E_z(r,z)\, \exp(i\,\omega\, z/c)$
    voltage with phase factor $\exp(i\,\omega\ z/c)$
- Loss parameter, R/Q, Q-value
  - $k_{\parallel}(r) = |V(r)|^2\,/(4\,U)$, (V/C)
  - $\frac{R}{Q} = 2\,k_{\parallel}(r)/\omega$,(Ohm)
  - Q-value (field distribution & conductivity of the wall) $Q = \omega\, U/P_{sur}$

A basic post-processing step is used to obtain the electric and magnetic field energy U and the voltage $V(r)$ at the radial position r. In a second step the loss parameter of the mode, the R/Q and the Q-value are calculated. P_{sur} is the power dissipated into the cavity wall due to the surface resistivity R_{sur}. In the MAFIA post-processor the dissipated power P_{sur} is often calculated for a copper surface with resistivity:

$$R_{Cu} = \sqrt{\frac{\omega\ \mu_0}{2\ \sigma_{Cu}}}, \qquad \sigma_{Cu} = 5.8 \cdot 10^7\ (\Omega\,\mathrm{m})^{-1}. \tag{16}$$

The Q-value of any material can be found by scaling the value for copper:

$$Q_{Mat} = \sqrt{\frac{\sigma_{Mat}}{\sigma_{Cu}}} Q_{Cu}, \tag{17}$$

where σ_{Mat} is the conductivity of the material. For steel the conductivity is approximately [20] $\sigma_{St} = 1.5 \cdot 10^6\ (\Omega\,\mathrm{m})^{-1}$. A purely geometric property of the chamber is the parameter G_1 [21], which is defined as:

$$G_1 \quad = \quad R_{Cu}\, Q_{Cu}. \tag{18}$$

In the next two subsections the results for the monopole and dipole modes are listed in Tab. 7, 8, 9 and 10. and are complemented with several plots of the electric fields.

3.1 Monopole Modes

The beam can only interact with TM-modes since the longitudinal electric field is identical to zero for TE-modes, i.e. the loss parameter is identically zero for TE-modes. Therefore only TM-monopole modes are considered in this subsection. The monopole mode with the lowest frequency of 751.0 MHz (EE-1) is trapped at the end of the End-cap-pipe about 10 m from the interaction point. The electric field of that mode is shown in Fig. 13, while the electric field of mode EE-2 (f = 786.6 MHz) is plotted in Fig. 14 also in the region between 9 m to 11 m from the IP.

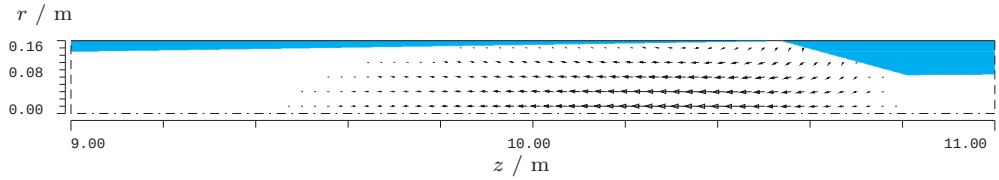

Figure 13: The electric field of mode EE-1 in the CMS vacuum chamber.

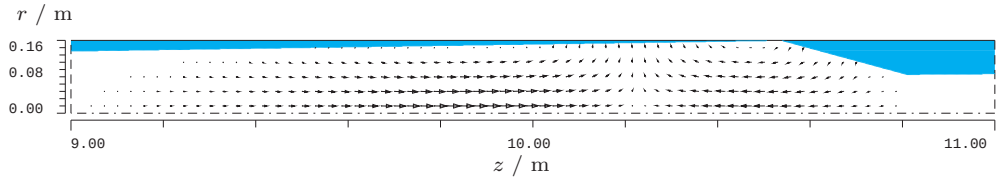

Figure 14: The electric field of mode EE-2 in the CMS vacuum chamber.

The basic rf-parameters of all modes are summarized in Tables 7 and 8.

Mode	f / MHz	$k^{(0)}$ /(V/nC)	G_1 / Ohm	R/Q / Ohm	Q_{Cu}	Q_{Steel}
EE-1	750.9	0.362	450.3	0.153	62980	10128
EE-2	786.5	0.306	458.5	0.124	62660	10076
EE-3	816.3	0.266	465.1	0.104	62402	10035
EE-4	843.1	0.236	471.0	0.089	62178	9999
EE-5	868.0	0.212	476.5	0.078	61988	9968
EE-6	891.5	0.190	481.5	0.068	61807	9939
EE-7	914.0	0.172	486.3	0.060	61656	9915
EE-8	935.6	0.155	490.8	0.053	61501	9890
EE-9	956.6	0.139	495.3	0.046	61380	9870
EE-10	977.0	0.128	499.4	0.042	61243	9848
EE-11	996.8	0.118	503.5	0.038	61127	9830
EE-12	1016.2	0.115	507.5	0.036	61027	9814
EE-13	1035.2	0.114	511.2	0.035	60899	9793
EE-14	1053.8	0.121	514.8	0.036	60783	9774
EE-15	1072.1	0.135	518.5	0.040	60696	9760
EE-16	1090.0	0.154	521.8	0.045	60578	9741
EE-17	1107.8	0.181	524.9	0.052	60446	9720
EE-18	1125.2	0.212	528.2	0.060	60352	9705
EE-19	1137.7	3.136	440.7	0.877	50079	8053
EE-20	1142.5	0.241	531.3	0.067	60244	9688
EE-21	1159.6	0.273	534.5	0.075	60160	9674
EE-22	1171.3	2.605	447.3	0.708	50091	8055
EE-23	1176.6	0.302	537.3	0.082	60039	9655
EE-24	1193.5	0.321	540.5	0.085	59971	9644
EE-25	1199.2	2.320	452.1	0.616	50043	8047
EE-26	1210.2	0.331	543.6	0.087	59893	9631
EE-27	1224.1	2.122	456.2	0.552	49979	8037
EE-28	1226.9	0.344	547.0	0.089	59856	9625
EE-29	1243.5	0.346	550.1	0.089	59793	9615
EE-30	1247.0	1.968	459.8	0.502	49909	8026
EE-31	1259.9	0.345	553.0	0.087	59720	9603
EE-32	1268.7	1.848	463.1	0.464	49840	8015
EE-33	1276.3	0.337	556.0	0.084	59656	9593
EE-34	1289.3	1.723	466.4	0.425	49786	8006
EE-35	1292.5	0.451	558.3	0.111	59525	9572

Table 7: Monopole modes of the CMS vacuum chamber.

Mode	f / MHz	$k^{(0)}$ /(V/nC)	G_1 / Ohm	R/Q / Ohm	Q_{Cu}	Q_{Steel}
EE-36	1308.2	1.417	528.2	0.345	55979	9002
EE-37	1309.4	0.796	495.6	0.193	52493	8441
EE-38	1324.2	0.296	553.3	0.071	58282	9372
EE-39	1328.9	1.217	483.4	0.292	50822	8173
EE-40	1340.1	0.414	558.1	0.098	58432	9396
EE-41	1349.0	1.878	495.3	0.443	51687	8312
EE-42	1356.8	1.078	557.7	0.253	58031	9332
EE-43	1371.8	1.949	527.9	0.452	54691	8795
EE-44	1375.3	1.421	537.3	0.329	55532	8930
EE-45	1387.5	0.206	558.2	0.047	57442	9237
EE-46	1396.5	0.482	529.8	0.110	54342	8739
EE-47	1405.5	0.263	561.0	0.060	57364	9225
EE-48	1418.3	0.318	556.9	0.071	56702	9118
EE-49	1426.9	1.347	547.3	0.301	55553	8933
EE-50	1445.2	1.462	569.8	0.322	57630	9267

Table 8: Monopole modes of the CMS vacuum chamber.

The loss parameters of the monopole modes from Tables 7 and 8 are plotted versus the mode frequency in Fig. 15.

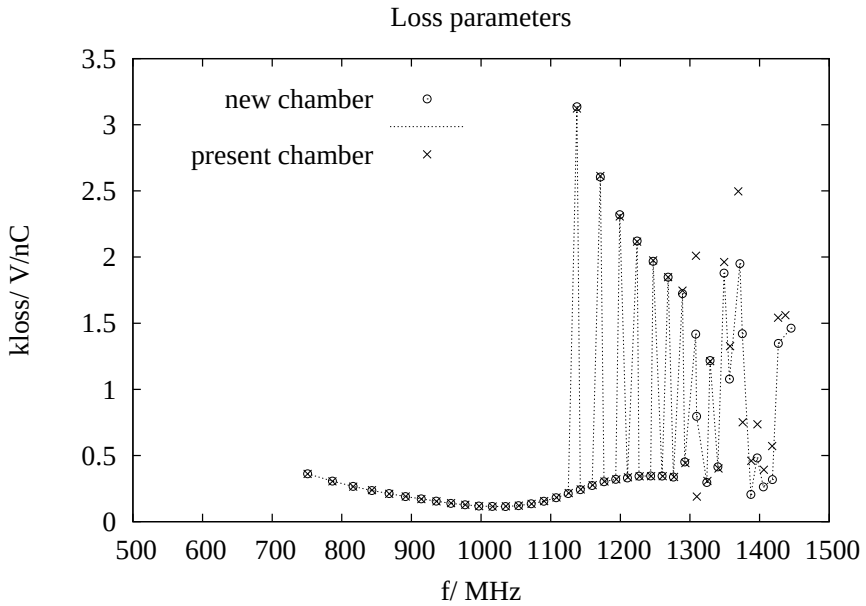

Figure 15: A plot of the loss parameters of the monopole modes versus frequency using the data from Tables 7 and 8. The data points are marked with circles. (The dotted line is intended only to guide the eye.) The loss parameters of the present geometry from Ref. [7] are also plotted (crosses).

In addition the loss parameters of the present geometry from Ref. [7] are also plotted in Fig. 15. The difference is small for most of the modes since the geometry is unchanged in the region where most of the modes are trapped.

If a mode is resonantly excited the power loss in that mode will be

$$P_{res} = \frac{1}{2} R_s \, {I_{tot}}^2, \tag{19}$$

where R_s is the effective shunt impedance of the mode and I_{tot} is the total beam current. For the HL-LHC the total beam current is about a factor of two larger than the nominal beam current of the LHC from Ref. [2], see Tables 1 and 2. Since the resonant power loss scales with the square of the total beam current the potential resonant power loss will be a factor 4 larger compared to the previously obtained results in Ref. [7].

3.2 Dipole Modes

The beam interacts with dipole modes only in the case that the beam traverses the CMS vacuum chamber off axis since the longitudinal electric field of any dipole mode vanishes on axis. The loss parameters of dipole modes have been calculated for an offset of $r = 1$ cm from the axis of the vacuum chamber. From the loss parameters the $R^{(1)}/Q$ parameter and the transverse impedance were obtained using the following relations:

$$\frac{R^{(1)}}{Q} = \frac{1}{r^2} \frac{2\, k_{\parallel}(r)}{\omega}, \tag{20}$$

$$Z_{\perp} = \frac{1}{\omega/c} \frac{R^{(1)}}{Q} Q_{Steel}. \tag{21}$$

The units of $R^{(1)}/Q$ and for $Z_{\perp}$ are Ohm/m^2 and Ohm/m respectively. A summary of the data of the dipole modes are given in Tables 9 and 10.

The dipole mode with the lowest frequency of 583.9 MHz (EE-1) is trapped at the end of the End-cap-pipe about 10 m from the interaction point. The electric field is shown in Fig. 16. The mode EE-16 with a frequency of 882.5 MHz is trapped in the HF-pipe (see Fig. 17).

Mode	f / MHz	$k^{(0)}$ /(V/nC)	G_1 / Ohm	R/Q / Ohm	Q_{Cu}	Q_{Steel}
EE-1	583.9	10.5	261.772	41522	6677	3.11
EE-2	616.3	11.5	273.327	42200	6786	3.12
EE-3	643.6	12.4	282.921	42747	6874	3.13
EE-4	668.1	12.9	291.724	43221	6950	3.06
EE-5	691.1	13.4	299.293	43639	7017	2.10
EE-6	712.8	13.8	306.701	44033	7081	2.93
EE-7	733.5	13.9	313.638	44387	7138	2.80
EE-8	753.6	13.8	320.274	44719	7191	2.65
EE-9	773.0	13.7	326.604	45026	7240	2.51
EE-10	792.0	13.5	332.787	45326	7289	2.38
EE-11	810.5	13.4	338.563	45583	7330	2.26
EE-12	828.6	13.3	344.435	45863	7375	2.18
EE-13	846.5	13.4	349.954	46104	7414	2.10
EE-14	864.0	14.1	355.295	46330	7450	2.13
EE-15	881.3	15.1	360.780	46581	7491	2.21
EE-16	882.5	29.1	254.527	32840	5281	2.10
EE-17	898.4	16.8	365.974	46800	7526	2.38
EE-18	913.0	31.9	261.569	33180	5335	3.10
EE-19	915.3	18.9	370.848	46984	7555	2.59
EE-20	932.0	21.9	375.812	47185	7588	2.91
EE-21	938.5	34.3	267.333	33448	5379	3.18
EE-22	948.5	25.3	380.618	47371	7618	3.26
EE-23	961.3	37.9	272.520	33690	5417	3.37
EE-24	964.8	28.4	384.679	47470	7633	3.54
EE-25	980.8	29.2	383.238	46904	7542	3.47

Table 9: Dipole modes of the CMS vacuum chamber.

Mode	f / MHz	$k^{(0)}$ /(V/nC)	G_1 / Ohm	R/Q / Ohm	Q_{Cu}	Q_{Steel}
EE-26	982.5	40.1	279.893	34226	5504	3.48
EE-27	996.6	38.5	385.068	46754	7518	4.43
EE-28	1002.6	49.2	286.820	34720	5583	4.15
EE-29	1012.2	64.6	385.572	46453	7470	7.15
EE-30	1022.1	69.3	307.942	36919	5937	5.98
EE-31	1028.6	9.3	381.324	45572	7328	0.98
EE-32	1040.8	8.3	355.246	42206	6787	0.79
EE-33	1047.6	36.6	358.720	42481	6831	3.46
EE-34	1058.8	46.3	388.372	45749	7357	4.62
EE-35	1068.6	58.3	365.915	42904	6899	5.35
EE-36	1077.5	108.6	393.742	45977	7393	10.50
EE-37	1088.9	111.6	396.565	46063	7407	10.58
EE-38	1098.5	75.6	391.580	45286	7282	6.93
EE-39	1108.4	58.2	411.003	47318	7609	5.48
EE-40	1119.7	55.1	411.855	47177	7586	5.07
EE-41	1129.6	19.3	412.855	47084	7571	1.74
EE-42	1139.9	1.1	425.897	48352	7775	0.10
EE-43	1151.1	2.8	428.755	48438	7789	0.25
EE-44	1161.4	22.8	430.969	48472	7795	2.00
EE-45	1171.6	37.4	442.776	49583	7973	3.30
EE-46	1182.2	8.7	540.158	60215	9683	0.92
EE-47	1183.9	60.6	552.065	61500	9890	6.49
EE-48	1193.7	80.8	449.075	49820	8011	6.90
EE-49	1204.1	120.5	457.165	50499	8121	10.25
EE-50	1215.2	116.5	462.594	50865	8179	9.80

Table 10: Dipole modes of the CMS vacuum chamber.

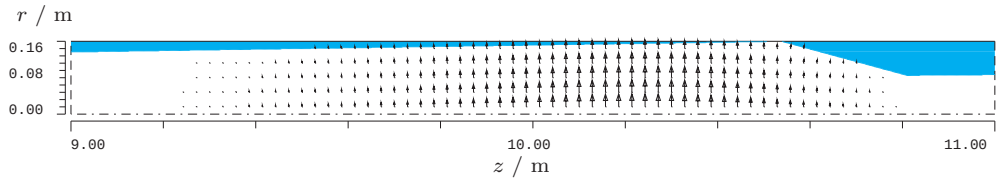

Figure 16: The electric field of dipole mode EE-1 in the CMS vacuum chamber.

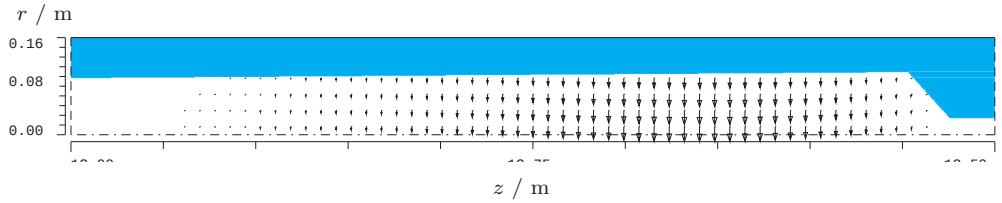

Figure 17: The electric field of dipole mode EE-16 in the CMS vacuum chamber.

The loss parameters of the dipole modes from Tables 9 and 10 at a radius $r = 1$ cm are plotted versus the mode frequency in Fig. 18. For comparison the corresponding loss parameters of the present geometry from Ref. [7] are also plotted. The differences are small.

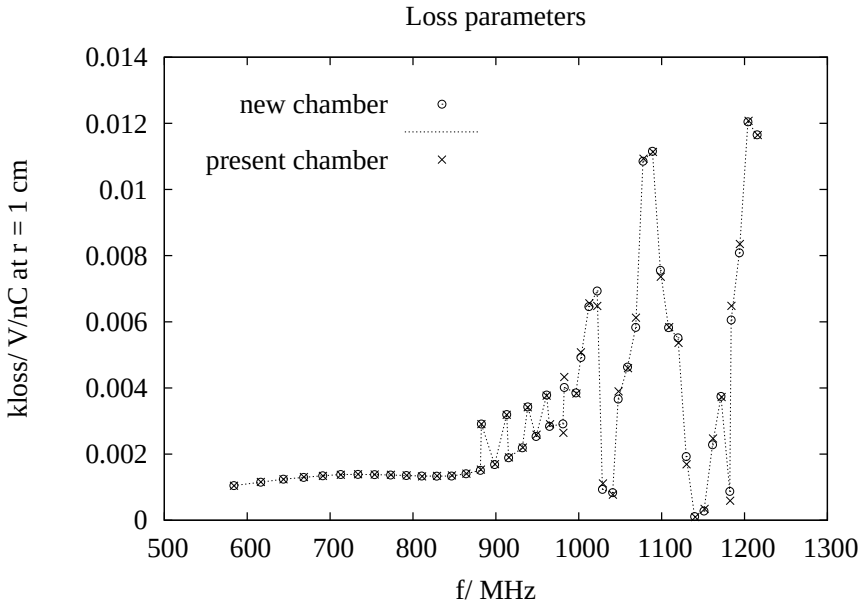

Figure 18: Plot of the loss parameters of the dipole modes at an offset of $r = 1$ cm versus frequency using the data from Tables 9 and 10. The data points are marked with circles. (The dotted line is intended only to guide the eye.) The loss parameters of the present geometry from Ref. [7] are also plotted (crosses).

4 Conclusion

The wakefields and higher order modes of the new beam pipe of the CMS detector for the High Luminosity LHC configuration (HL-LHC) have been calculated with the ECHO2D [10, 11] and MAFIA [18, 17] using a 2D model of the vacuum chamber. The radius of the central beam pipe is 21.7 mm for the new design while the presently installed chamber has a radius of 29.0 mm.

A comparison with results for the new design and previously obtained results [7, 8] for the present chamber shows a slight increase of the transverse impedance while the longitudinal loss parameter is almost not affected by the design change provided that the rms bunch length is $\sigma_z = 7.5$ cm, see Tables 4 and 5. This situation changes dramatically if a shorter rms bunch length of only $\sigma_z = 4.0$ cm is considered. The transverse impedance is a factor two larger for the shorter bunch (4 cm) compared to a bunch with a length of 7.5 cm (rms). More important is the much larger (factor 19) loss parameter (see Table 6). The transient power loss can be more than 2 kW for the parameter option 2 of Table 2.

The loss parameters of the monopole modes (see Fig. 15) and the corresponding parameters for the dipole modes (Fig. 18) of the new chamber do not differ much from the loss parameters of the present geometry [7] since the geometry is unchanged in the region where most of the modes are trapped.

Acknowledgment

The research leading to these results has received funding from the European Commission under the FP7 project HiLumi LHC, GA no. 284404.

We would like to thank Elias Métral for his skill in providing a good collaboration environment within the Task 2.4 on impedance issues and collective effects which he leads. Thanks go to Bernhard Holzer, Daniel Pitzl, Benoit Salvant and Wolfram Zeuner who helped us obtain all the details about the new design of the CMS vacuum chamber. Last but not least we would like thank Mark Lomperski for carefully reading the manuscript.

References

[1] O. Brüning, H. Burkhardt, S. Myers, *The Large Hadron Collider*, Progress in Particle and Nuclear Physics, Volume 67, Issue 3, July 2012, Pages 705-734

[2] O. Brüning (ed.), P. Collier (ed.), P. Lebrun (ed.), S. Myers (ed.), R. Ostojic (ed.), J. Poole (ed.), P. Proudlock (ed.), *LHC Design Report - Vol 1 the LHC Main Ring*, CERN-2004-003-V-1, 2004.

[3] O. Brüning, *Loss Factor and Longitudinal Higher Order Modes in the CMS Experimental Chamber*, CERN, LHC Project Note 14, October 1995.

[4] O. Brüning, *Longitudinal and transverse Modes in the CMS Experimental Chamber*, CERN, LHC Project Note 36, March 1996.

[5] O. Brüning, *Coherent Losses in the CMS Experimental Chamber*, CERN, LHC Project Note 63, March 1996.

[6] D. Angal-Kalinin, *Review of Coupled Bunch Instabilities in the LHC*, CERN, LHC Project Note 595, July 2002.

[7] R. Wanzenberg, *Calculation of Higher Order Modes and Wakefields for the Vacuum Chamber of the CMS Experiment at the LHC*, CERN, LHC Project Note 418, May 2009.

[8] E. Metral and R. Wanzenberg, *Wake and Higher Order Mode Computation for CMS Experimental Chamber at the LHC*, Proceedings of 2009 Particle Accelerator Conference, PAC09, Vancouver, Canada, May 4-8, 2009, and CERN-ATS-2009-118

[9] A. Ball, *Beampipe design/approval/procurement*, Pix meeting, Aug. 2011

[10] I. Zagorodnov and T. Weiland, *TE/TM field solver for particle beam simulations without numerical Cherenkov radiation*, Phys. Rev. ST Accel. Beams **8** (2005) 042001.

[11] I. Zagorodnov, *Indirect methods for wake potential integration*, Phys. Rev. ST Accel. Beams **9** (2006) 102002 [arXiv:physics/0606049].

[12] T. Weiland, R. Wanzenberg, *Wakefields and Impedances*, in: Joint US-CERN part. acc. school, Hilton Head Island, SC, USA, 7 - 14 Nov 1990 / Ed. by M Dienes, M Month and S Turner. - Springer, Berlin, 1992- (Lecture notes in physics ; 400) - pp.39-79.

[13] W.K.H. Panofsky, W.A. Wenzel, *Some consideration concerning the transverse deflection of charged particles in radio-frequency fields* , Rev. Sci. Inst. Vol 27, 11 (1956), 967.

[14] M. Dohlus, private communication (2008).

[15] T. F. Günzel, *Transverse Coupling Impedance Of The Storage Ring At The European Synchrotron Radiation Facility*, Phys. Rev. ST Accel. Beams **9** (2006) 114402.

[16] A. Novokhatski and T. Weiland, *Inductive impedance and longitudinal instability*, Proceedings of the 7th European Particle Accelerator Conference (EPAC 2000), Vienna, Austria, 26-30 Jun 2000.

[17] T. Weiland, *On the numerical solution of Maxwell's Equations and Applications in the Field of Accelerator Physics*, Part. Acc. 15 (1984), 245-292.

[18] *MAFIA Release 4 (V4.200)* CST AG, Bad Nauheimer Str. 19, 64289 Darmstadt, Germany.

[19] T. Weiland, *On the computation of resonant modes in cylindrically symmetric cavities*, NIM 216 (1983) 329-348.

[20] D.R. Lide, Ed. *Handbook of Chemistry and Physics* , 79th edition, 1998-1999, CRC Press, Washington, D.C.

[21] P.B. Wilson *High Energy Electron Linacs: Application to Storage Ring RF Systems and Linear Colliders*, AIP Conference Proceedings 87, American Institute of Physics, New York (1982),p. 450-563.